

Article

Research on the Control Algorithm of Coaxial Rotor Aircraft based on Sliding Mode and PID

Yiran Wei ¹ , Han Chen ², Kewei Li ¹, Hongbin Deng ^{1,*} and Dongfang Li ^{1,3}

¹ School of Mechatronical Engineering, Beijing Institute of Technology, Beijing 100081, China; 3120195081@bit.edu.cn (Y.W.); likewei@bit.edu.cn (K.L.); 3120150135@bit.edu.cn (D.L.)

² Interdisciplinary Division of Aeronautical and Aviation Engineering, The Hong Kong Polytechnic University, Hong Kong 999077, China; stark.chen@connect.polyu.hk

³ School of Computer Science and Technology, Shandong University of Technology, Zibo 255000, China

* Correspondence: denghongbin@bit.edu.cn; Tel.: +86-185-1129-3398

Received: 16 October 2019; Accepted: 28 November 2019; Published: 29 November 2019



Abstract: In this paper, a sliding mode PID control algorithm of coaxial rotor aircraft has been proposed. After that, Adams/MATLAB simulation and experiments were used for verification. The results show that this control method can achieve satisfactory results. Firstly, when considering of the aerodynamic interaction between upper and lower rotor, it is difficult to establish an accurate mathematical model, and the aerodynamic interference between the upper and lower rotors and the brandishing motion of the blades are calculated by using the blade element theory and the dynamic inflow model, and the other parts which are not accurately modeled are compensated for by the control algorithm. Secondly, the sliding mode control algorithm and the PID control algorithm are combined to control the attitude of the aircraft. Among them, the PID control algorithm is used to establish the relationship between attitude and position, so that the aircraft can fly and hover more steadily. Thirdly, the three-dimensional model of the aircraft was imported into Adams to establish the dynamic simulation model. Then, the controller was established in Simulink, after that, and then the controller and the dynamic simulation model were combined for joint simulation. And the sliding mode PID control algorithm has been compared with traditional PID control algorithm through the simulation. Finally, the sliding mode PID control algorithm is verified by the experiment compared with the traditional PID algorithm. The results verify the superiority and practicability of the control method designed in this paper.

Keywords: coaxial rotor aircraft; control algorithm; hover; joint simulation; experiment

1. Introduction

In recent years, more and more scientists and engineers have been paying attention to Unmanned Aerial Vehicles (UAVs), especially micro-UAVs. Micro-rotors are more flexible than full-size helicopters. Their compact size and ability to hover, turn, and move in all directions make small rotor aircraft ideal for operating in dynamic environments. Compared with fixed-wing aircraft, a micro-rotor aircraft has significant advantages, especially in the need to retain the aircraft position at rest (hovering) or in a strictly restricted environment. Micro-rotor UAVs can perform a variety of tasks, such as reconnaissance of the environment, medical rescue, communication relay, and so on [1].

Because of its advantages in maneuverability, versatility, stability, and ease of control, and considering the actual project requirements, this paper focuses on the configuration of a coaxial rotor aircraft rather than a single rotor. Comparing the coaxial rotor aircraft with the most popular Four-rotor aircraft, the structure of the coaxial rotor aircraft is more compact than the four-rotor aircraft. Despite the existence of some foldable four-rotor aircraft, the feature size of the coaxial rotor aircraft

involved in this paper is significantly reduced, being more portable and suitable for use. The coaxial rotor aircraft we chose is being developed independently by our laboratory. The maximum takeoff weight is about 8 kg and the rotor diameter is about 28 inches. After folding, the size of the fuselage is less than 120 mm in diameter and the full length is about 100 cm. It is placed in a narrow and long rocket compartment for transportation and delivery, and the folded rotor is simpler and more reliable than the folded fuselage design [2].

Compared with other kinds of aircrafts, the research on coaxial rotor aircraft is relatively less. Automatic Control Laboratory of Tlemcen presented a nonlinear control method based on sliding mode control (SMC) for the position and the attitude tracking control of a small coaxial-rotor UAV subjected to uncertainties and aerodynamic disturbances [3]. Recently, they proposed a hierarchical controller based on a new disturbance observer with finite time convergence to solve the path tracking of a small coaxial-rotor-typs UAVs despite unknown aerodynamic efforts [4], however, the advanced algorithms they studied are still only at the simulation level, without experimental verification. There is still a long way to go before engineering applications; the French-German Research Institute of Saint-Louis presented a comprehensive design of a Gun Launched Micro Air Vehicle (GLMAV) which is a new Micro Air Vehicle (MAV) concept using two-bladed coaxial contra-rotating rotors and a cyclic swashplate. The nonlinear model of this kind of coaxial rotor aircraft in hovering and flight was studied in detail [5,6]. After four years of research and development, a full functional prototype of a GLMAV system was designed, manufactured, and tested [7], however, due to the lack of an appropriate control algorithm, it is difficult for the GLMAV to achieve good flight stability and control accuracy. Other universities like Maryland and Duke University have mainly studied small coaxial dual-rotor helicopters and made outstanding contributions to their structure optimization [8,9].

This paper is mainly aimed at the control algorithm of the coaxial rotor aircraft. In this research field, Arama (Purdue University) has designed a hybrid control strategy for a coaxial rotor aircraft, and the simulation results are satisfactory [10]. However, the control algorithm does not fully exploit the advantages of the hybrid control strategy and needs further improvement. Espinoza et al. proposed a control algorithm implemented on the embedded system, and the simulation and experimental results show the good performance of the developed system during the flight [11], but they only carried out desktop experiments on the designed controller. Whether the designed controller can be applied to the aircraft they proposed and achieve the expected effect need to be further verified. Husnic at Drexel University in the United States designed the controller for a kind of coaxial rotor aircraft and used MATLAB/Flightgear to carry out joint simulation [1]. Furthermore, in order to make the simulation more convincing, some specific experiments need to be done. Li at the Beijing Institute of Technology studied the application of a decoupling algorithm in the control of coaxial rotor aircraft [12], however the control algorithm is too complicated to be applied to the specific engineering problem.

Although some control algorithms for coaxial rotor aircraft have been proposed, most of the algorithms are only in the theoretical and simulation stages, and there are few algorithms verified by experiments. Regarding controller design and simulation technology, relevant research at home and abroad is based on the simplified or approximate kinetic model of the coaxial rotor aircraft to design the control algorithm. The performance of the control algorithm is tested on the MATLAB/Simulink simulation platform. There are two problems in this practice. Firstly, the problem of upper and lower rotor disturbances can only be solved using empirical formulas and approximate theory [13,14]. The magnitude and direction of thrust under different system conditions cannot be accurately judged before the prototype test, and the system error still exists in the model. If the controller is highly dependent on the model, even if good results can be achieved in the simulation, the attitude divergence will be caused by unmodeled errors, assembly and machining accuracy, steering accuracy, and other problems in the prototype experiment [15]. In addition, it is difficult to accurately model the complex control mechanism of the aircraft in MATLAB. Current simulation methods are based on simplified mathematical models, which consider the aircraft as a rigid body with external control forces, ignoring the relative motion of the components. Without establishing the relationship between the actuator

maneuver and the control output of the control algorithm, there is a big gap between the controller output and the actual situation [7].

Motivated by the above discussion, this paper mainly achieves innovation in the following three aspects. Firstly, the sliding mode and PID control algorithm with better adaptability and robustness is applied to the coaxial rotor aircraft with complex control actuators, which makes the attitude control more rapid and stable. Secondly, the Adams/MATLAB joint simulation technology is applied to the aircraft control simulation to solve the difficult problem of mathematical modeling and numerical simulation of the UAV with a complex control mechanism. Joint simulation technology can be used to better model the dynamic system of the actual aircraft, including the steering gear and its transmission mechanism, so the reliability is higher [16]. This makes the simulation in this paper reliable and effective and has the advantages of visualization. At last, the prototype is used for experimental test, then the mathematical model, control algorithm and simulation results of the aircraft are further verified, which fully demonstrates the superiority and feasibility of the control algorithm designed in this paper.

This paper is organized as follows: In Section 2, according to the self-developed coaxial rotor aircraft, flight control principle is introduced. In Section 3, the modeling and derivation processes are given. The controller design based on the sliding mode PID control algorithm is described in Section 4. After that, the simulation results are shown in Section 5. Finally, flight experiment and data analysis are shown in Section 6.

2. Flight Control Principle

The coaxial rotor aircraft involved in this paper is composed of the mission load, battery compartment, fuselage, lower rotor, upper rotor, and so on. All the 3D models of the structure are completed in SolidWorks, as shown in Figures 1 and 2.

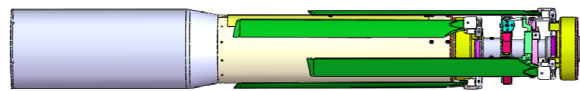


Figure 1. The coaxial rotor aircraft with rotors folded.

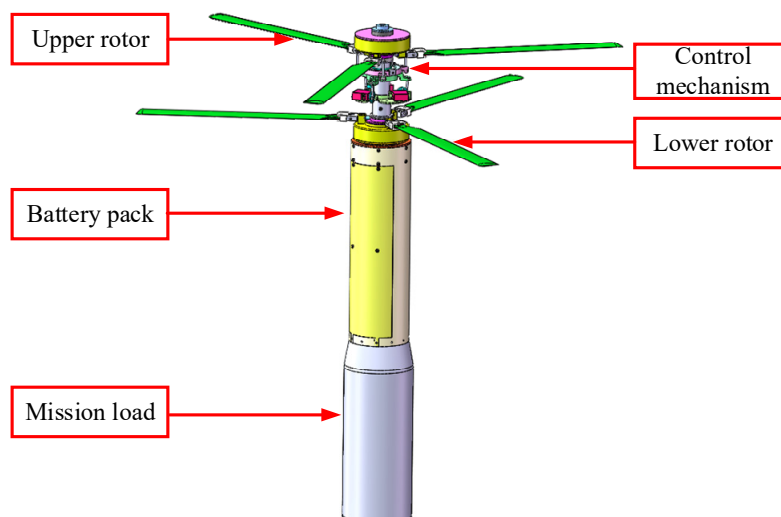


Figure 2. The coaxial rotor aircraft structure composition.

The battery compartment and task load can be regarded as the load of the aircraft, and they are connected with the body. The blades of the upper and lower paddles can be folded. When flying, the aircraft reaches the horizontal position by centrifugal force, and the activity range of the swing

hinge is about 120 degrees. The following is a description of the principle of steering control on the fuselage, as shown in Figure 3.

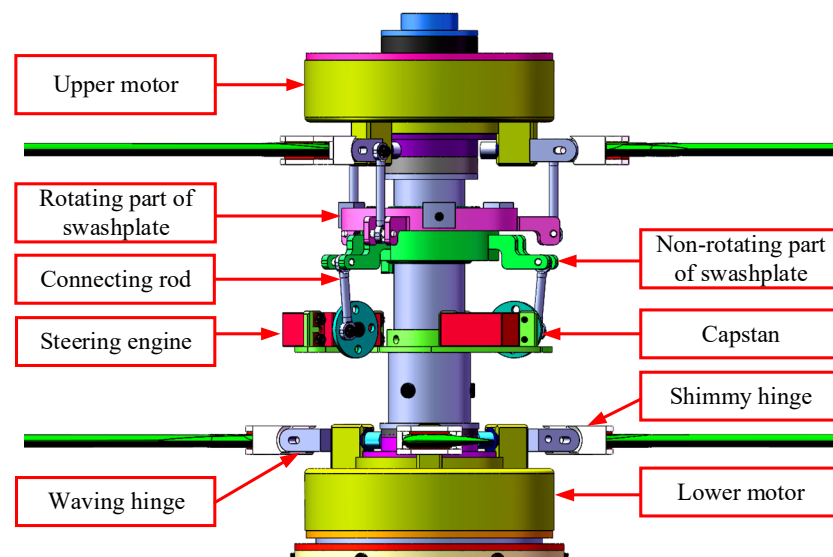


Figure 3. The control mechanism.

All ends of the connecting rod in Figure 3 are constrained by spherical joints. The brushless motor drives the capstan and connecting rod to connect with the upper swashplate. There is a spherical bearing in the swashplate, which makes the center point coincide with the central axis of the aircraft and can tilt and move up/down the axis. According to the geometric principle, the position of the three points in space can determine a plane, and the tilt angle of the swashplate can be completely determined by the three steering gears. When the normal vector of the swashplate plane does not coincide with the central axis of the fuselage, the angle of attack of the upper blade varies periodically. During the rotation of the blade, the attack angle of the connecting rod corresponds to the attitude of the steering ring. The angle of the attack at the lower ring of the swashplate will increase, and the thrust will also increase. When the swashplate is higher, the opposite is true. The result is that the resultant thrust direction of all blades produced by the upper paddle is the same as the normal vector direction of the swashplate plane [17].

When the craft flies forward, the blade will start to swing. This kind of motion is more complex, which will bring challenges to the controller design. The aircraft involved in this paper restricts the amplitude of the flapping motion and reduces its influence via structural design. In the next kinetic modeling, we consider the problem of periodic pitch caused by the flapping motion. The approximate method is used for modeling, while the sliding mode control is used to solve the problem of modeling inaccuracy [18].

3. Aircraft Kinetic Model

3.1. Model without Rotor Interference or Flapping Motion

To facilitate the modeling, two coordinate systems are introduced: The earth coordinate system E-xyz and the body coordinate system B-xyz, as shown in Figure 4. The E coordinate system can be regarded as the inertial coordinate system, while the B coordinate system is the airframe coordinate system, and the origin of B is located at the centroid of the aircraft.

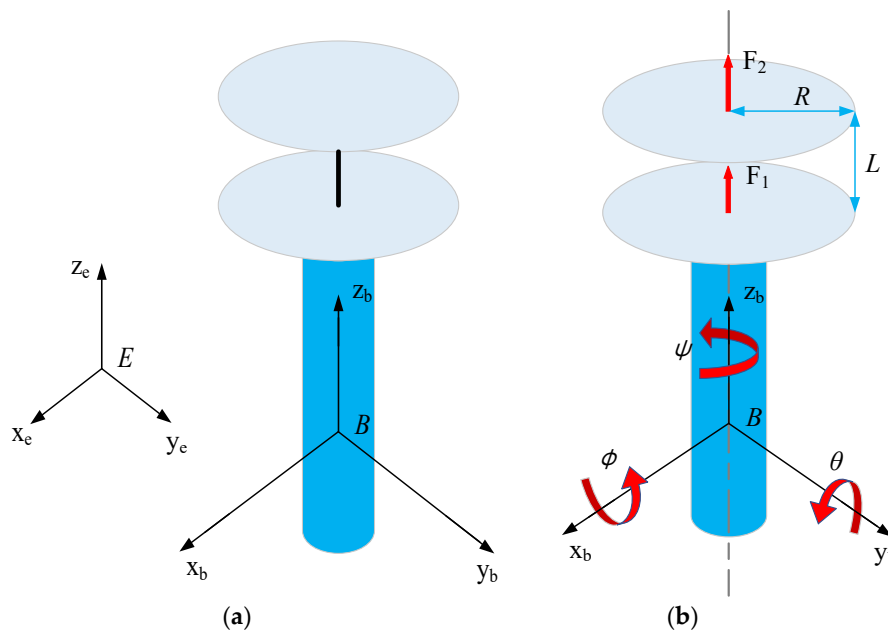


Figure 4. (a) The aircraft's coordinate system and (b) simplified model.

In order to facilitate analysis, we must ensure that the research results are effective. The following assumptions are made:

- (1) The whole coaxial rotor aircraft is regarded as a rigid body.
- (2) The centroid of the coaxial rotor aircraft is considered to coincide with the central symmetry axis.
- (3) Because of the small volume and mass of the rotor, the gyroscopic effect of the rotor can be neglected [18].

$V = (p, q, r, u, v, w)$ is defined as the velocity vector of the body, which is the velocity vector of the coaxial rotor aircraft in the body coordinate system. p, q, r are the aircraft stability derivatives due to roll rate, pitch rate, yaw rate, respectively. u, v, w are the aircraft stability derivatives due to longitudinal velocity, lateral velocity, vertical velocity, respectively. $\eta = (\varphi, \theta, \psi)^T$ represents the attitude angle vector of the coaxial rotor aircraft. Among the angles, φ, θ, ψ represent the roll angle, pitch angle, and yaw angle. $X = (x, y, z)^T$ represents the spatial position vector of the centroid of the coaxial rotor aircraft in the earth coordinate system. m is the mass of the aircraft, and I_x, I_y and I_z are the moments of inertia of the aircraft, respectively.

Based on Euler-Poincare equation, the kinetic model of the coaxial rotor aircraft is established. The general form of the equation is as follows:

$$M(Q)\dot{V} + C(Q, V)V = F(V, Q, U) \tag{1}$$

where Q is the generalized coordinate vector of the body centroid relative to the Earth coordinate system. U is the control force; $M(Q)$ is inertia matrix. $C(Q, V)$ is a transformation matrix derived from the Euler dynamic equation, and $F(V, Q, U)$ is the sum of the aerodynamic in the body coordinate system, gravitational, and control inputs. $V(Q)$ is the matrix to transform the body coordinates of the rotorcraft to the earth coordinate system. The direction of F is defined as going straight up. In order

to simplify writing, writes $s() = \sin()$, $c() = \cos()$ and the specific expressions of partial matrices in Equation (1) are as follows:

$$M(Q) = \begin{bmatrix} I_x & 0 & 0 & 0 & 0 & 0 \\ 0 & I_y & 0 & 0 & 0 & 0 \\ 0 & 0 & I_z & 0 & 0 & 0 \\ 0 & 0 & 0 & m & 0 & 0 \\ 0 & 0 & 0 & 0 & m & 0 \\ 0 & 0 & 0 & 0 & 0 & m \end{bmatrix} \tag{2}$$

$$C(Q, V) = \begin{bmatrix} 0 & -I_y r & I_z q & 0 & 0 & 0 \\ I_x r & 0 & -I_z p & 0 & 0 & 0 \\ -I_x q & I_y p & 0 & 0 & 0 & 0 \\ 0 & 0 & 0 & 0 & 0 & 0 \\ 0 & 0 & 0 & 0 & 0 & 0 \\ 0 & 0 & 0 & 0 & 0 & 0 \end{bmatrix} \tag{3}$$

$$V(Q) = \begin{bmatrix} c\theta c\psi & s\phi s\theta c\psi - c\phi s\psi & c\phi s\theta c\psi + s\phi s\psi & 0 & 0 & 0 \\ c\theta s\psi & s\phi s\theta s\psi + c\phi c\psi & c\phi s\theta s\psi - s\phi c\psi & 0 & 0 & 0 \\ -s\theta & s\phi c\theta & c\phi c\theta & 0 & 0 & 0 \\ 0 & 0 & 0 & c\theta c\psi & s\phi s\theta c\psi - c\phi s\psi & c\phi s\theta c\psi + s\phi s\psi \\ 0 & 0 & 0 & c\theta s\psi & s\phi s\theta s\psi + c\phi c\psi & c\phi s\theta s\psi - s\phi c\psi \\ 0 & 0 & 0 & -s\theta & s\phi c\theta & c\phi c\theta \end{bmatrix} \tag{4}$$

The thrust direction of the upper rotor can be changed within a certain range under the control of the steering gear. The projection of F_2 in the $yo z$ and xoz planes is shown in Figure 5. The coordinates of the output shaft of the steering gear in the xoy plane are $(x_1, y_1)(x_2, y_2)(x_3, y_3)$ in sequence. The displacement of the actuator on the output shaft of the actuator is z_1, z_2, z_3 . Assuming that the distance between the thrust plane and the origin of the coordinate system is D at the initial position $z_1 = z_2 = z_3 = 0$, the thrust plane must pass through three points: $(x_1, y_1, D+z_1)(x_2, y_2, D+z_2)$ and $(x_3, y_3, D+z_3)$. These can form three directional vectors, perpendicular to F_2 . The F_2 direction vector can be expressed as $\left(\frac{F_{2x}}{F_2}, \frac{F_{2y}}{F_2}, \sqrt{1 - \left(\frac{F_{2x}}{F_2}\right)^2 - \left(\frac{F_{2y}}{F_2}\right)^2}\right)$ in the body coordinate system. According to the vector's vertical relations, the equation can be listed as follows:

$$\begin{cases} \frac{F_{2x}}{F_2}(x_2 - x_1) + \frac{F_{2y}}{F_2}(y_2 - y_1) + \sqrt{1 - \left(\frac{F_{2x}}{F_2}\right)^2 - \left(\frac{F_{2y}}{F_2}\right)^2}(z_2 - z_1) = 0 \\ \frac{F_{2x}}{F_2}(x_3 - x_1) + \frac{F_{2y}}{F_2}(y_3 - y_1) + \sqrt{1 - \left(\frac{F_{2x}}{F_2}\right)^2 - \left(\frac{F_{2y}}{F_2}\right)^2}(z_3 - z_1) = 0 \end{cases} \tag{5}$$

The F_{2x}, F_{2y} in the formula are the projections of F_2 on the x and y axes in the body coordinate system. Let z_1 be used as a benchmark for adjusting the total pitch and thrust of the upper rotor system to vary with the F_2 expected value of the controller output. Then, z_2 and z_3 can be solved.

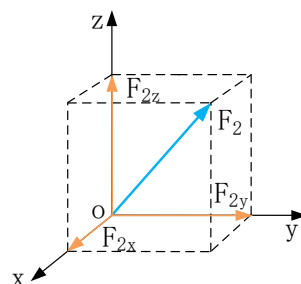


Figure 5. Decomposition of the upper rotor thrust.

The force condition of aircraft centroid is given by Equation (6):

$$F(v, q, u) = \begin{bmatrix} U_2 D \\ U_3 D \\ U_4 \\ U_3 \\ U_2 \\ U_1 \end{bmatrix} + V(Q) \begin{bmatrix} 0 \\ 0 \\ 0 \\ 0 \\ 0 \\ -mg \end{bmatrix} \tag{6}$$

$$\begin{cases} U_1 = F_1 + F_{2z} \\ U_2 = F_{2y} \\ U_3 = F_{2x} \\ U_4 = \eta(F_1 - F_2) \end{cases} \tag{7}$$

In the formula, U_1 is the vertical height of the control variable, U_2 is the roll input control variable, U_3 is the pitch control input, U_4 is the yaw control variable, and η is the rotary torque coefficient, which is related to the resistance of the rotor and the friction coefficient of the motor shaft.

According to the blade-element theory, we assume that the angle of attack is a fixed value. The thrust of the rotor is established by the following Equation (8):

$$F = \int_0^R \frac{1}{2} \alpha \rho d_l(x) C_T x^2 \Omega^2 dx \tag{8}$$

where α is the blade section angle of attack. ρ is the air density. $d_l(x)$ is a function of blade chord length (blade element length) varying with blade element position, which is related to blade shape. C_t is the thrust coefficient of the rotor. Ω is the rotor rotational speed.

According to Equations (6) and (7), the time derivative of the Earth coordinate system can be obtained:

$$\ddot{Q} = \begin{cases} -(-I_y \dot{\theta} \dot{\psi} + I_z \dot{\theta} \dot{\psi} - D U_2) / I_x, \\ -(-I_x \dot{\phi} \dot{\psi} + I_z \dot{\phi} \dot{\psi} - D U_3) / I_y, \\ -(-I_x \dot{\phi} \dot{\theta} + I_y \dot{\phi} \dot{\theta} - U_4) / I_z, \\ [c\phi c\theta U_3 + (s\phi c\psi s\theta - c\phi s\psi) U_2 + U_1 (c\phi c\psi s\theta + s\phi s\psi)] / m, \\ [s\psi c\theta U_3 + (s\phi s\psi s\theta + c\phi c\psi) U_2 + U_1 (c\phi s\psi s\theta - s\phi c\psi)] / m, \\ (-s\theta U_3 + s\phi c\theta U_2 + U_1 c\phi c\theta) / m - g. \end{cases} \tag{9}$$

When the coaxial rotor aircraft flies at low speed without wind or with very low wind speed, the influence of air drag on the system is small and can be neglected. At the same time, assuming that the roll angle and pitch angle of coaxial rotor aircraft in flight are very small, and the rate of change is also small enough, the mathematical model of the system can be simplified as follows:

$$\begin{cases} \ddot{\phi} = \frac{D U_2}{I_x} & \ddot{\theta} = \frac{D U_3}{I_y} & \ddot{\psi} = \frac{U_4}{I_z} \\ \ddot{x} = [U_3 c\phi c\theta + (s\phi c\psi s\theta - c\phi s\psi) U_2 + U_1 (c\phi c\psi s\theta + s\phi s\psi)] / m \\ \ddot{y} = [U_3 s\psi c\theta + (s\phi s\psi s\theta + c\phi c\psi) U_2 + U_1 (c\phi s\psi s\theta - s\phi c\psi)] / m \\ \ddot{z} = (-U_3 s\theta + U_2 s\phi c\theta + U_1 c\phi c\theta) / m - g \end{cases} \tag{10}$$

It can be seen from the above formula that the coupling between the three channels of the altitude and horizontal position of the aircraft is very prominent. Considering the influence of the aerodynamic interaction between the rotor blades on the inflow dynamics, the dynamic process regarding force and torque is more complicated. Beyond the nonlinearity of the aircraft body dynamics, it superimposes the prominent nonlinearity of the control process, aggravating the coupling problem.

3.2. The Model with Rotor Interference and Flapping Motion

In order to reflect the aerodynamic interference between the upper and lower rotor blades, based on blade-element theory and the Pitt-Peters dynamic inflow model, the disturbances of the upper and lower rotor inflow and flapping motion models are established. Compared with the eddy theory, or CFD method, this method has advantages of simplicity and convenience with respect to calculation and is in good agreement with the experimental data. Notably, the model is based on the following assumptions: The blade is considered to be rigid; the truncation effect at the blade root, tip loss, and flapping hinge extension is neglected, and the unsteady effect is neglected; the inflow velocity is considered to be uniformly distributed in the plane of the blade disk [17]. The core idea is to link the induced dynamic speed and the air resistance change through the following formula:

$$M_i \dot{\lambda}_{in} + V_m L^T \lambda_{in} = C \tag{11}$$

The $\lambda_{in} = (\lambda_0, \lambda_s, \lambda_c)^T$ in the formula indicates the time-averaged, 1 order transverse, and 1 order longitudinal components of the induced inflow ratio. $C = (C_T, C_l, C_m)^T$ shows rotor thrust, roll moment, and pitch moment coefficients. M_i , V_m , and L are the inertia matrix, mass flow parameter matrix, and static transfer matrix of inflow dynamics, respectively. The interaction of the induced velocity is expressed by the following formula:

$$\lambda_i = \lambda_{0,i} + K_{ji} \lambda_{0,j} + \lambda_{fs}, \quad (i, j \in \{u, l\}, i \neq j) \tag{12}$$

K_{ji} represents the induced velocity interference coefficient between rotor pairs, which is related to design parameters such as the diameter and spacing of the two rotor pairs.

According to the above inflow interference model, the tension and torque of the rotor system can be expressed as follows:

$$\begin{cases} T = k_6(C_{Tu} + C_{Tl}) & \dot{\lambda}_{0,i} = k_4(-k_1\theta_i + k_2\lambda_{0,i}\lambda_i + k_3\lambda_i) \\ Q = k_8(C_{Qu} - C_{Ql}) & \lambda_{fs} = \frac{w}{\Omega R} \\ C_{Ti} = k_5(\frac{1}{3}\theta_i - \frac{1}{2}\lambda_i) & \lambda_{0,i} = \frac{v_{0,i}}{\Omega R} \\ C_{Qi} = \lambda_i C_{Ti} + k_7 C_d & \lambda_{0,j} = \frac{v_{0,j}}{\Omega R} \\ \lambda_i = \lambda_{0,i} + K_{ji} \lambda_{0,j} + \lambda_{fs} \end{cases} \tag{13}$$

$$k_1 = \frac{\sigma a}{45}, k_2 = \frac{4}{15}, k_3 = \frac{\sigma a}{30}, k_4 = \frac{-45\pi\Omega}{16}, k_5 = \frac{\sigma a}{2}, k_6 = \rho A \Omega^2 R^2, k_7 = \frac{\sigma}{8}, k_8 = k_6 R \tag{14}$$

$\sigma = (N_b c) / (\pi R)$ stands for the authenticity of the rotor disk, c is the blade chord, N_b stands for the number of blades on the rotor disk, and a is the blade section two-dimensional lift-curve slope. A is the rotor disk area, C_d is the section drag coefficient, w is the projection of the mass velocity of an aircraft in the body coordinate system B along the Z axis, ρ is the air density, λ indicates the rotor inflow ratio, $\lambda_{0,i}$ is the inflow ratio to a blade from infinity, $v_{0,i}$ is the induced velocity of a blade from infinity, and θ_i is blade pitch angle. T and Q are the thrust and torque generated by the whole rotor system. l represents the lower rotor, and u corresponds to the upper rotor. In addition, if the stiffness of the blade is considered, the orthogonal moments of flapping motion for the pitch and roll channels are [19]:

$$M_x = k_9 \alpha_b, M_y = k_9 \alpha_a \tag{15}$$

Among them, $k_9 = N_b S_\beta \gamma I_b \Omega^2 / 8$. γ is the blade Lock number, S_β is the stiffness coefficient of the blade, I_b is the flapping moment of inertia, α_a is the longitudinal angle of flapping, and α_b is the

lateral angle of flapping. In summary, after considering the flapping motion and rotor aerodynamic interference, the kinetic model of the coaxial rotor aircraft (other terms remain unchanged) is modified to:

$$\begin{cases} F_1 = k_6 C_{Tl} \\ F_2 = k_6 C_{Tu} \\ U_4 = Q \end{cases} \tag{16}$$

$$\ddot{\phi} = \frac{DU_2}{I_x} + M_x, \ddot{\theta} = \frac{DU_3}{I_y} + M_y$$

4. Controller Design

4.1. Overall Control Structure

Figure 6 is a schematic diagram of the control structure of a coaxial rotor aircraft system. The whole control system can be divided into attitude control and position control.

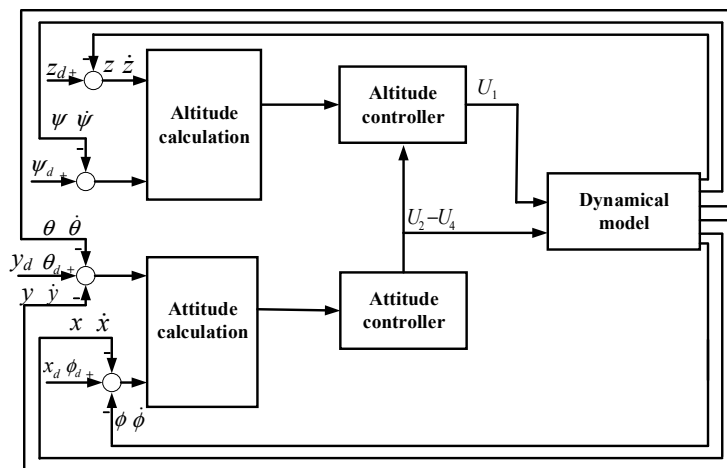


Figure 6. The control structure.

There is no coupling relationship between the three-axis attitude controls of the coaxial rotor aircraft, and the attitude control response is the fastest. Therefore, priority is given to control the attitude to ensure precise control, considering the underactuated problem of the coaxial rotor aircraft: 4 inputs control and 6 degrees of freedom. First, the mathematical relationship between the attitude angle and the horizontal position is established directly through the PID algorithm. The information of the desired attitude angle can be calculated through the horizontal position information, and the height control volume is calculated according to the attitude angle and horizontal control. The purpose of trajectory tracking can then be achieved by controlling attitude angle and position height [20,21]. The expected values of roll angle and pitch angle are as follows:

$$\begin{cases} \phi_d = k_{p2}(Y_d - Y) + k_{i2} \int (Y_d - Y)dt + k_{d2}(\dot{Y}_d - \dot{Y}) \\ \theta_d = k_{p1}(X_d - X) + k_{i1} \int (X_d - X)dt + k_{d1}(\dot{X}_d - \dot{X}) \\ \psi_d = 0 \end{cases} \tag{17}$$

In the formula, k_p , k_i , and k_d are the proportional, integral, and differential adjustment coefficients, respectively; φ_d , θ_d , and ψ_d are the desired pitch, roll, and yaw angles; X , Y can be measured by an airborne sensor.

4.2. Sliding Mode PID Control Algorithm

The sliding mode PID algorithm is based on the traditional sliding mode control algorithm to design a sliding mode surface function of PID [17]. This method has the advantages of robustness and fast response of the sliding mode algorithm, and can reduce the chattering problem of the sliding mode algorithm. When we do the simulation, we compare it with other commonly used control algorithms. We find that sliding mode PID works best, especially when disturbance is added. In addition, due to the complexity of the mechanical structure of the coaxial rotor aircraft, many unknown disturbances will be added to the prototype test. Combining the above factors, we choose sliding mode PID to design our algorithm.

The general design steps of the sliding mode controller are as follows: the first is to select the proper PID sliding surface function (s), and the second is to design the appropriate control law so that the system can reach and maintain the desired sliding surface, $s = 0$.

Taking the coaxial rotor aircraft pitching channel as an example, the tracking error is defined as:

$$e_\phi = \phi_d - \phi \tag{18}$$

Then we choose the sliding surface function, as follows:

$$s_\phi = \dot{e}_\phi + \lambda_1 e_\phi + \lambda_2 \int e_\phi dt, \lambda_1, \lambda_2 > 0 \tag{19}$$

We next derive the control law equation according to the reaching law and select the exponential reaching law.

$$\dot{s}_\phi = -\varepsilon \text{sgn}(s_\phi) - ks_\phi \tag{20}$$

In the formula, \dot{s}_ϕ is the derivative of s_ϕ to time; ε and k are normal numbers; $\varepsilon = 0.2, k = 1$ and sgn is the symbolic function. Select the Lyapunov function as follows:

$$V_\phi = \frac{1}{2} s_\phi^2 \tag{21}$$

so, we have:

$$\dot{V}_\phi = s_\phi \dot{s}_\phi = s_\phi [-\varepsilon \text{sgn}(s_\phi) - ks_\phi] = -\varepsilon \|s_\phi\| - k \|s_\phi\|^2 < 0 \tag{22}$$

It is shown that the control system is asymptotically stable, and the tracking error finally converges to 0, which satisfies the reachability condition of the sliding mode:

$$\dot{s}_\phi = \ddot{e}_\phi + \lambda_1 \dot{e}_\phi + \lambda_2 e_\phi = \ddot{\phi}_d - \left(\frac{DU_2}{I_x} + M_x\right) + \lambda_1 \dot{e}_\phi + \lambda_2 e_\phi = -\varepsilon \text{sgn}(s_z) - ks_z \tag{23}$$

We can thus get:

$$U_2 = \frac{I_x}{D} [\ddot{\phi}_d + \varepsilon \text{sgn}(s_\phi) + c_1 \dot{e}_\phi + c_2 e_\phi + ks_\phi - M_x] \tag{24}$$

Similarly, the control law of the roll angle, yaw angle, and height can be obtained as follows:

$$\begin{aligned} U_3 &= \frac{I_y}{D} [\ddot{\theta}_d + \varepsilon \text{sgn}(s_\theta) + d_1 \dot{e}_\theta + d_2 e_\theta + ks_\theta - M_y] \\ U_4 &= I_z [\ddot{\psi}_d + \varepsilon \text{sgn}(s_\psi) + h_1 \dot{e}_\psi + h_2 e_\psi + ks_\psi] \\ U_1 &= \frac{1}{c\phi c\theta} \{m[g + \ddot{z}_d + \varepsilon \text{sgn}(s_z) + \lambda_1 \dot{e}_z + \lambda_2 e_z + ks_z] + s\theta U_3 - s\phi c\theta U_2\} \end{aligned} \tag{25}$$

In this formula, $c_1, c_2, d_1, d_2, h_1, h_2$ are positive constants.

5. Joint Simulation of Adams/MATLAB

5.1. Simulation Model Establishment

We conceive of putting the model of aircraft into Adams and establishing a relationship with the control model of MATLAB. In the simulation, the calculation process of the control algorithm is controlled by MATLAB, and the control process and results are presented in the Adams environment. In this way, the flight state of the aircraft can be simulated, and the animation effect can be formed. The current attitude and position of the aircraft can be seen very intuitively.

First, we need to simplify the assembly built in Solidworks. According to the relative motion relation, combine components that do not move relative to each other during flight into a single part. After simplification, we import these parts into Adams View to add the constraint relationship, force, and torque, and set the input and output variables. Finally, we can get the kinetic model file. Because Adams does not have the ability to simulate aerodynamics, the induced velocity, blade drag coefficient, and yaw angle in the formula are derived from the aerodynamic simulation and experiment of the model. Then the acting points of the tension and torque of the two rotors are placed in the center of the propeller disk. The value of force is defined in the form of the function shown by Formula 11.

The output file of the kinetic model in Adams will be read by Simulink. After opening, the kinetic model relates to the control model built in Simulink. Its output is the three attitude angles and centroid space coordinates of the aircraft. The next step is to establish the relationship between the input and output of the dynamic module through the control algorithm in Simulink. In MATLAB/Simulink, modules are assembled into controllers, and appropriate custom functions are added. Because of the information about the mass and moment of inertia of the aircraft in the control law, it is necessary to initialize the information before the program runs. In this paper, we use the method of running m file to write all the initialized constants into the same file and then upload them to the workspace. After running the Simulink models, they can be produced. This is convenient for unified revision and management and is simpler than other methods [22]. The whole simulation model is completed as shown in Figure 7.

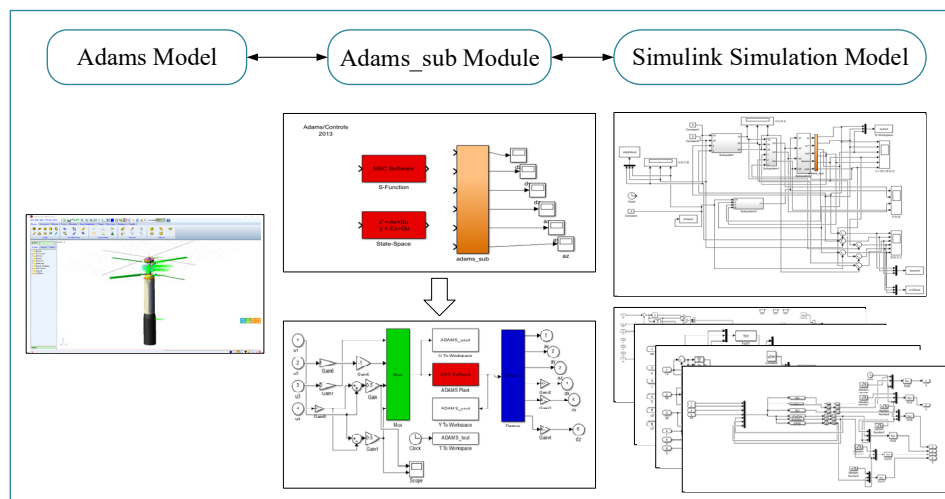


Figure 7. The simulation model in Adams & Simulink.

The input to the aircraft kinetic model is three steering angles θ_1 , θ_2 and θ_3 , and the rotational speed Ω_u and Ω_l . The three steering gears are the same type, and the two electric motors are the same. Their internal response problems are not considered. The relationship between the four control

variables ($U_1 - U_4$) has been established. Next, in order to transform the relationship, we designed some rules to convert $U_1 - U_4$ into $\theta_1, \theta_2, \theta_3, \Omega_u, \Omega_l$, totaling five inputs:

$$\begin{cases} \theta_1 = \frac{z_1}{\Delta z_1} \Delta\theta & \Omega_l = \sqrt{\frac{F_1}{C_{Tl}\rho AR^2}} \\ \theta_2 = \frac{z_2}{\Delta z_2} \Delta\theta & z_1 = \frac{U_1 \Delta z_1}{3mg} \\ \theta_3 = \frac{z_3}{\Delta z_3} \Delta\theta & F_2 = \frac{1}{2} \left(U_1 + \frac{U_4}{\lambda_i R} \right) + \frac{U_2^2 + U_3^2}{U_1 + \frac{U_4}{\lambda_i R}} \\ \Omega_u = \sqrt{\frac{F_2}{C_{Tu}\rho AR^2}} & F_1 = F_2 - \frac{U_4}{\lambda_i R} \end{cases} \quad (26)$$

Among them, $\Delta z_1, \Delta z_2, \Delta z_3$ represent the displacement range of the z-axis caused by the position of the lifting surface corresponding to the output shaft of the three steering gears. The $\Delta\theta$ is the rotation range of the corresponding steering gear. Together with Equation (5), five inputs can be calculated.

5.2. Hovering Simulation Results

The initial value of the system simulation is X_0 , and the vector is defined as follows:

$$X_0 = [0, 0, 0, 0, 0, 0, 0, 0, 0, 0, 0, 0]$$

where, the numbers from left to right are the position of the system x, y, and z, attitude angles, φ, θ, ψ , velocity of x, y, z axis, and angular velocity of x, y, z axis, in sequence. All the initial values of the system are 0. The parameters in the controller are drawn from a certain range according to the fixed step size, as shown in Table 1. Gradually reducing the scope and step length determines the best parameters. After adjustment, a group of better results was selected.

Table 1. Controller parameter list.

Parameter	Value	Parameter	Value
k_{p1}	7.32	λ_2	0.13
k_{i1}	0.03	c_1	15.86
k_{d1}	25	c_2	7.1
k_{p2}	8.35	d_1	8.3
k_{i2}	0.02	d_2	2.42
k_{d2}	28	h_1	4
λ_1	0.85	h_2	1

The structural dimensions and aerodynamic parameters of the aircraft are shown in Table 2.

Table 2. Aircraft dynamics parameters.

Parameter	Value
Aircraft Mass m	8.636 kg
Acceleration due to gravity g	9.8 m/s ²
Distance from centroid to upper rotor L	0.518 m
Rotor thrust coefficient C_T	0.0033
Rotor solidity σ	0.065
blade section lift-curve slope a_0	0.12
Induced velocity $v_{0,i}, v_{0,j}$	7.98 m/s, 16.57 m/s
Rotor radius R	0.385 m
Air density ρ	1.29 kg/m ³
Aircraft roll moment of inertia I_x	0.786 kg.m ²
Aircraft pitch moment of inertia I_y	0.786 kg.m ²
Aircraft yaw moment of inertia I_z	0.079 kg.m ²

The induced velocity field is not actually evenly distributed in space. It is also related to rotor speed, and only average values are taken here. When the target position coordinates are set and the initial position is different, set the target position coordinates as (3, 3, 3). The simulated 3-D trajectory, position, and attitude change curves with time and animation screenshots are shown in Figures 8–10.

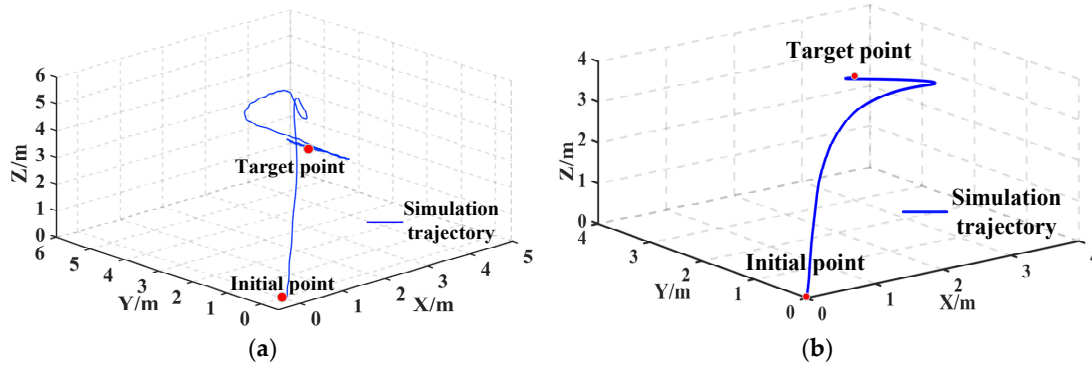


Figure 8. The move-hover trajectory of traditional PID control and sliding mode PID control. (a) Traditional PID control; (b) Sliding mode PID control.

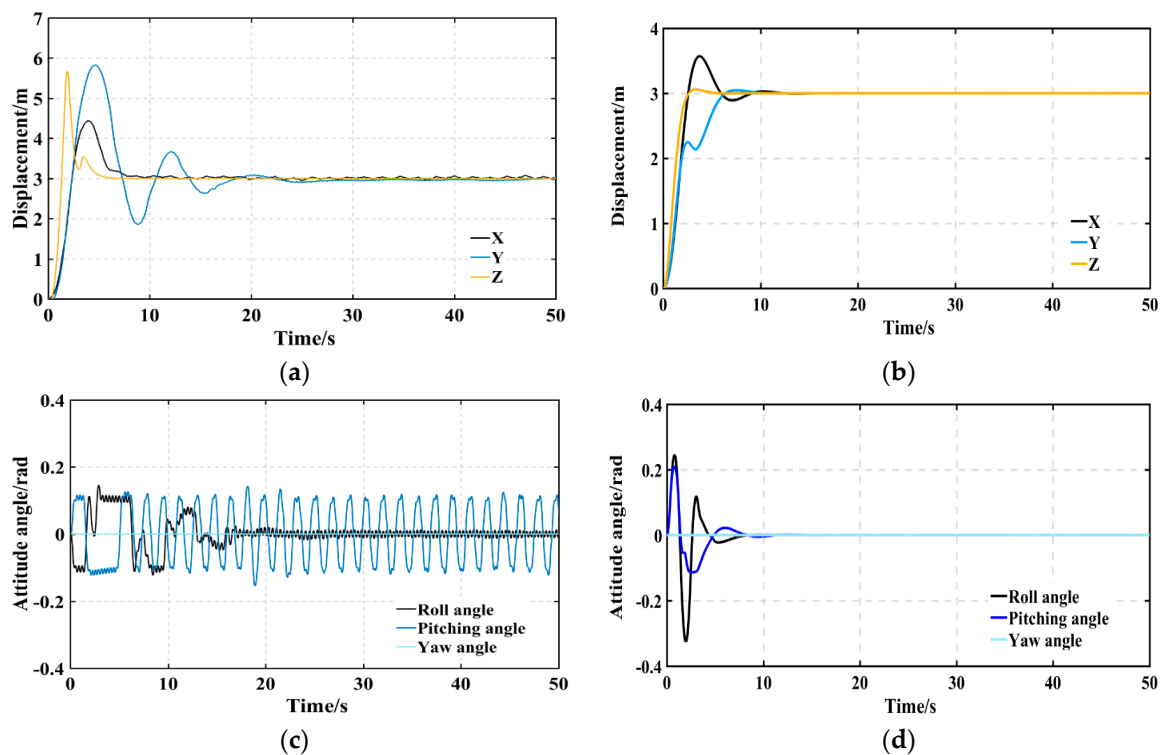


Figure 9. Move-hover simulation results of traditional PID control and sliding mode PID control. (a) Displacement of traditional PID control; (b) Displacement of sliding mode PID control; (c) Attitude angle of traditional PID control; (d) Attitude angle of sliding mode PID control.

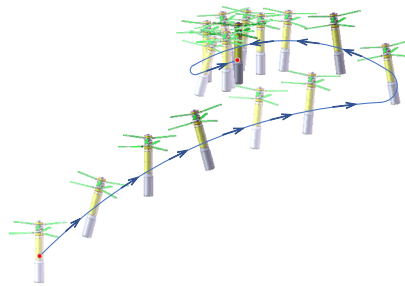


Figure 10. The move-hover animation screenshots of sliding mode PID control algorithm.

Comparing the trajectories of the coaxial rotor aircraft under the traditional PID control algorithm and the sliding mode PID control algorithm, the aircraft started from the same initial point to the target point, as shown in Figure 8. Under the control of the traditional PID, the aircraft can fly from the initial point to the target point, the flight path is wobbly, the controllability is not high, and the stability is poor, as shown in Figure 8a. Under the control of the sliding mode PID, the aircraft has experienced only one turn from the starting point to the target point, with smooth flight path and high controllability and stability, as shown in Figure 8b.

The displacement and attitude angle from the same initial point to the target point are compared under the traditional PID control algorithm and sliding mode PID control algorithm, as shown in Figure 9. In order to achieve its own stability, sliding mode PID has a shorter regulation time than traditional PID in the case of the same overshoot. Under the control of the traditional PID, the aircraft vibrates many times after reaching the peak time, as shown in Figure 9a; while under the control of the sliding mode PID, the aircraft enters into the regulation time soon after reaching the peak time, reaching a stable state, as shown in Figure 9b. At the same time, under the control of the traditional PID, the aircraft will vibrate in a relatively small range after reaching a stable state. Such vibration cannot be gradually stabilized by using the system, as shown in Figure 9c; under the control of the sliding mode PID, although the aircraft has large vibration in the previous period. But after a very short time, the system will gradually become stable, as shown in Figure 9d.

It can be seen from the Figure 10, after a short initial overshoot and vibration, the controller can still be stable near the target position, indicating that the controller designed in this paper meets the necessary requirements.

6. Experiments

In order to verify the feasibility and practicability of the sliding mode PID control algorithm proposed in this paper, it is necessary to apply the algorithm to the prototype aircraft for experimental test. The prototype aircraft is manufactured with the model structure diagram proposed in Section 2, as shown in Figure 11. The working principle of the control mechanism is that, under the control of the input signal of the steering gear, the rotating ring of swashplate and the non-rotating ring are tilted together in the corresponding direction. Since the rotating ring relates to the fixed length of the rod between the pitch hinges of the blade, the tilt of the tilter causes the pitch of the blade to change periodically, making the rotor aerodynamically asymmetrical, and the rotor vertebral body will tilt in the corresponding direction. The direction of the tension vector of the rotor is also inclined in the corresponding direction, to achieve the purpose of maneuvering the aircraft in lateral and longitudinal flight.

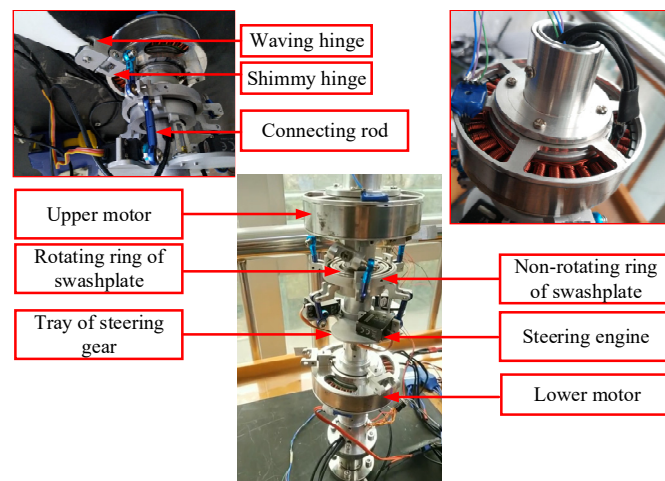


Figure 11. Schematic diagram of control mechanism.

Figure 12 shows the flight of the aircraft in the experimental. As Figure 12a is a satellite observation map, the resolution may not be high enough, from which we can see the trajectory of the aircraft from take-off point to hover point, and can be used as the basis for the authenticity of experimental data. Figure 12b shows the actual flight of the aircraft, indicating the flight process from takeoff to hover. As can be seen, the attitude of the aircraft is very stable during the flight.



Figure 12. Flight experiment. (a) Satellite image; (b) Photograph of the flight.

The variation of the attitude angle of the coaxial rotor aircraft under the traditional PID control algorithm and the sliding mode PID control algorithm during the flight test is shown in Figure 13. Under the control of sliding mode PID, the roll angle and pitch angle of the aircraft are controlled within ± 4 deg, as shown in Figure 13a. Under the control of traditional PID, the amplitude of the fluctuation of the roll angle and pitch angle is within ± 8 deg, as shown in Figure 13b. The fluctuation frequency and fluctuation amplitude of the roll angle and pitch angle under the sliding mode PID control algorithm are significantly smoother than those under the traditional PID control algorithm. The yaw angle of the aircraft is the rotation of the aircraft along its main axis. Under the traditional PID control algorithm, the yaw angle shows dramatic and frequent changes. Under the sliding mode PID control algorithm, the yaw angle change process is continuous, smooth and stable.

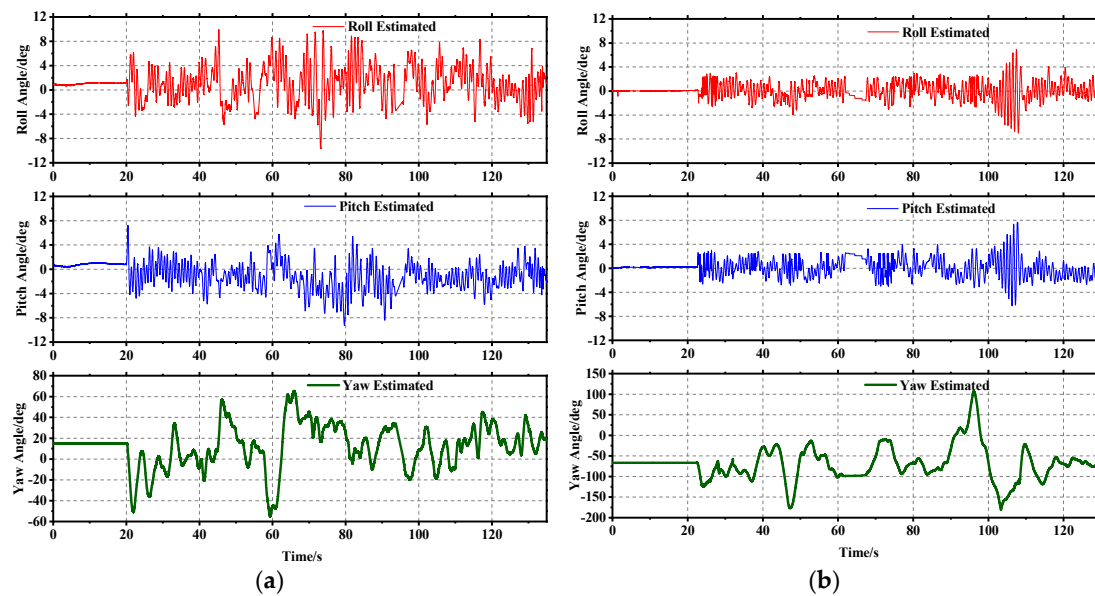


Figure 13. The attitude information of the aircraft. (a) Traditional PID control; (b) Sliding mode PID control.

The variation of the flight position of the coaxial rotor aircraft under the traditional PID control algorithm and the sliding mode PID control algorithm during the flight test is shown in Figure 14. The position curve of the aircraft under the sliding mode PID control algorithm is significantly smoother than that under the traditional PID control algorithm. Under the control of sliding mode PID, all of the directions of X, Y and Z, the position fluctuation of the aircraft is less than ± 0.3 m while ± 0.6 m under the control of traditional PID, which indicates that the aircraft has a small angle vibration, the flight is stable, and the aircraft is hovering steadily. In the process, the flight accuracy is high, and the fixed-point hover can be realized. However, in the process of flying at high altitude, vibration is inevitable, mainly because the aircraft's power system (motor, rotor) generates high-frequency vibration during the process of generating and transmitting power, and the surrounding environment (wind, magnetic field, etc.) will also affect the aircraft. It is acceptable to control this vibration within a certain range.

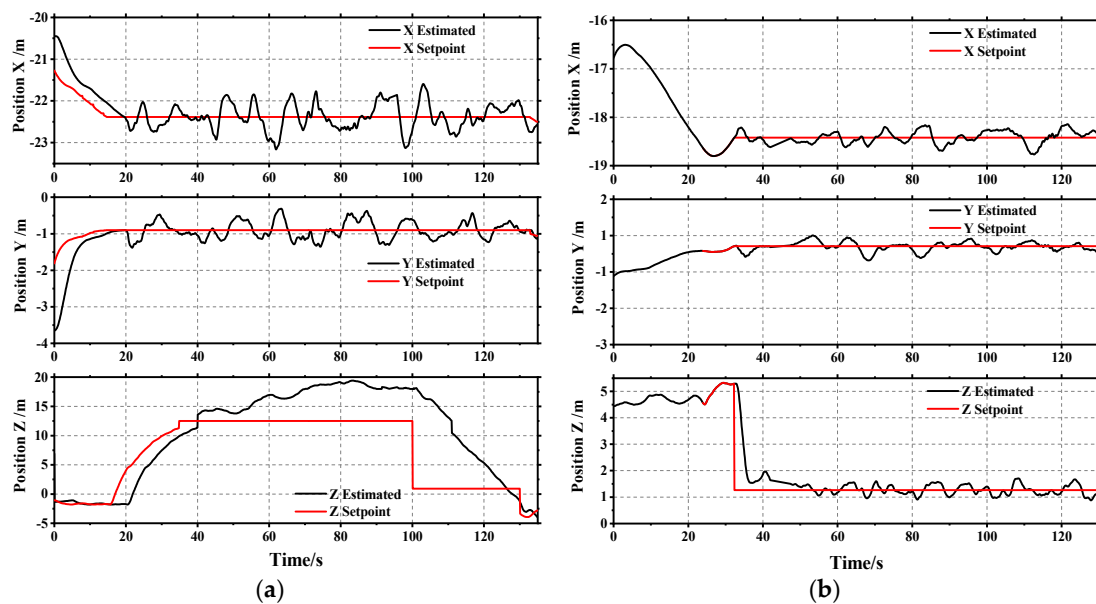


Figure 14. The position information of the aircraft. (a) Traditional PID control; (b) Sliding mode PID control.

7. Conclusions

A new coaxial rotor aircraft has been designed in this paper, then the kinematic model of the aircraft in the process of space motion is analyzed, and the dynamic model of aerodynamic interference and swing motion of the aircraft is established. In order to make the aircraft have a more stable flight path and attitude, a hybrid control algorithm based on sliding mode control and PID control is proposed. In order to verify the performance of the sliding mode PID control algorithm, simulations and experiments are carried out.

In the simulation part, the coaxial rotor aircraft model was imported into Adams for motion analysis and combined with the controller built in Simulink to conduct joint simulation. It can simulate the actual flight of aircraft very intuitively and effectively. Meanwhile, this keeps the control model in MATLAB very close to the actual flight control chip code, thus making the simulation results more credible. Then the sliding mode PID control algorithm is compared with the traditional PID control algorithm through simulation. The simulation results show that, under the control of sliding mode PID, the vibration amplitude of the trajectory and attitude of the aircraft is smaller, the convergence speed is faster, and the flight state is more stable. This kind of joint simulation can provide a way for future researchers to verify the control algorithm design in advance when there is no physical prototype.

In the experimental part, we made a prototype of the coaxial rotor aircraft, and applied these two control algorithms to the flight test on this platform. The experimental results and the simulation results are consistent within the allowable error range. The mutual confirmation further verifies the performance and simulation accuracy of the sliding mode PID control algorithm designed in this paper.

Finally, the superiority and feasibility of the control algorithm proposed in this paper are obtained. Under the control of sliding mode PID, the motion attitude and trajectory of the coaxial rotor aircraft are effectively controlled. The aircraft has good hovering stability and maneuverability, and the hovering performance meets the service requirements. Future work will explore and optimize the algorithm, when come across to unknown wind disturbance, the aircraft requires considerably posture adjustment and adapt to the flight environment, which is considered to be a more challenging issue.

Author Contributions: Conceptualization, data curation, project administration, resources, software, writing—review & editing, Y.W.; investigation, visualization, writing—original draft, H.C.; writing—original draft, K.L.; project administration, Resources, H.D.; methodology, Software, D.L.

Funding: This research received no external funding.

Acknowledgments: Thanks to Kewei Li for his help in experimental testing.

Conflicts of Interest: The authors declare no conflicts of interest.

References

1. Husnic, Z. Micro Coaxial Helicopter Controller Design. Ph.D. Thesis, Drexel University, Philadelphia, PA, USA, 2015.
2. Chen, M. Technology Characteristic and Development of Coaxial rotor aircraft Helicopter. *Aeronaut. Manuf. Technol.* **2009**, *17*, 26–31.
3. Mokhtari, M.R.; Cherki, B. Sliding mode control for a small coaxial rotorcraft UAV. In Proceedings of the 2015 3rd International Conference on Control, Engineering & Information Technology (CEIT), Tlemcen, Algeria, 25–27 May 2015; IEEE: Piscataway, NJ, USA, 2015.
4. Mokhtari, M.R.; Cherki, B.; Braham, A.C. Disturbance observer based hierarchical control of coaxial-rotor UAV. *ISA Trans.* **2017**, *67*, 466–475. [[CrossRef](#)]
5. Drouot, A.; Richard, E.; Boutayeb, M. Hierarchical backstepping-based control of a Gun Launched MAV in crosswinds: Theory and experiment. *Control Eng. Pract.* **2014**, *25*, 16–25. [[CrossRef](#)]
6. Roussel, E.; Gnemmi, P.; Changey, S. Gun-Launched Micro Air Vehicle: Concept, challenges and results. In Proceedings of the 2013 International Conference on Unmanned Aircraft Systems (ICUAS), Atlanta, GA, USA, 28–31 May 2013; IEEE: Piscataway, NJ, USA, 2013.
7. Gnemmi, P.; Changey, S.; Meder, K.; Roussel, E.; Rey, C.; Steinbach, C.; Berner, C. Conception and Manufacturing of a Projectile-Drone Hybrid System. *IEEE/ASME Trans. Mechatron.* **2017**, *22*, 940–951. [[CrossRef](#)]
8. Lee, T.E. Design and Performance of a Ducted Coaxial rotor aircraft in Hover and Forward Flight. Ph.D. Thesis, University of Maryland, College Park, MD, USA, 2010.
9. Giovanetti, E.B. Minimum Power Requirements and Optimal Rotor Design for Conventional, Compound, and Coaxial Helicopters Using Higher Harmonic Control. Ph.D. Thesis, Duke University, Durham, UK, 2013.
10. Arama, B. Design and Implementation of a Hybrid Control Strategy for a Small Scale Coaxial rotor aircraft Helicopter. Ph.D. Thesis, Purdue University, West Lafayette, IN, USA, 2011.
11. Espinoza, E.S.; Malo, A.; Lozano, R. Modeling and Sliding Mode Control of a Micro Helicopter-Airplane System. *J. Intell. Robot. Syst.* **2014**, *73*, 469–486. [[CrossRef](#)]
12. Li, K.; Wei, Y.; Wang, C.; Deng, H. Longitudinal Attitude Control Decoupling Algorithm Based on the Fuzzy Sliding Mode of a Coaxial-Rotor UAV. *Electronics* **2019**, *8*, 107. [[CrossRef](#)]
13. Bohorquez, F. Rotor Hover Performance and System Design of an Efficient Coaxial Rotary Wing Micro Air Vehicle. Ph.D. Thesis, Department of Aerospace Engineering, University of Maryland, College Park, MD, USA, 2007.
14. Wicha, J. Coaxial rotor aircraft Hover Power Reduction Using Dissimilarity between Upper and Lower Rotor Design. Ph.D. Thesis, Rensselaer Polytechnic Institute, Troy, NY, USA, 2015.
15. Xian, B.; Zhang, X.; Yang, S. Nonlinear controller design for an unmanned aerial vehicle with a slung-load. *Control Theory Appl.* **2016**. [[CrossRef](#)]
16. Wang, X.-L. C0-simulating Study on the Vehicle's Active Suspension Based on ADAMS and MATLAB. Ph.D. Thesis, Jilin University, Changchun, China, 2009.
17. Yuan, X.; Zhu, J.; Chen, Z.; Lu, X. Kinematic modeling and analysis of a coaxial helicopter's actuating mechanism. *Acta Aeronaut. Astronaut. Sin.* **2013**, *34*, 988–1000.
18. Liu, Y.-P.; Huang, X.-J.; Li, X.-Y. Trajectory Tracking Control of Quad-rotor Unmanned Aerial Vehicles based on Sliding Mode PID. *Mech. Sci. Technol. Aerosp. Eng.* **2017**, *36*, 1859–1865.
19. Johnson, W. Helicopter Theory. *Airf. Eng. Aerosp. Technol.* **2008**, *12*, 271–276.
20. Dong, Z.-Y. Research on Modeling and Control Algorithm for Unmanned Coaxial rotor aircraft Helicopter. Ph.D. Thesis, Jilin University, Changchun, China, 2016.

21. Chen, X.-Q. The Design & Research of the Flight Control System of Quadrotor. Ph.D. Thesis, Nanchang Hangkong University, Nanchang, China, 2014.
22. Shi, Y.Q.; Li, M.Y.; Dun, X.M.; Liu, Q. Coordinated Simulation of Biped Robot Based on ADAMS and Matlab. *Mach. Electron.* **2008**, *1*, 45–47.



© 2019 by the authors. Licensee MDPI, Basel, Switzerland. This article is an open access article distributed under the terms and conditions of the Creative Commons Attribution (CC BY) license (<http://creativecommons.org/licenses/by/4.0/>).